Journal of Robotics and Control (JRC)
Volume 4, Issue 6, 2023
ISSN: 2715-5072, DOI: 10.18196/jrc.v4i6.20071

A Passivity-based Control Combined with Sliding Mode Control for a DC-DC Boost Power Converter

Minh Ngoc Huynh [1,4], Hoai Nghia Duong [2*], Vinh Hao Nguyen [3]
[1, 3] Ho Chi Minh City University of Technology (HCMUT), Vietnam National University Ho Chi Minh City, Ho Chi Minh City, Vietnam
[2] Eastern International University, Binh Duong Province, Vietnam
[4] Industrial University of Ho Chi Minh City, Ho Chi Minh City, Vietnam
Email: [1] hmngoc.sdh20@hcmut.edu.vn, [2] nghia.duong@eiu.edu.vn, [3] vinhhao@hcmut.edu.vn
*Corresponding Author

Abstract—**In this paper, a passivity-based control combined with sliding mode control for a DC-DC boost power converter is proposed. Moreover, a passivity-based control for a DC-DC boost power converter is also proposed. Using a co-ordinate transformation of state variables and control input, a DC-DC boost power converter is passive. A new plant is zero-state observable and the equilibrium point at origin of this plant is asymptotically stable. Then, a passivity-based control is applied to this plant such that the capacitor voltage is equal to the desired voltage. Additionally, the sliding mode control law is chosen such that the derivative of Lyapunov function is negative semidefinite. Finally, a passivity-based control combined with sliding mode control law is applied to this plant such that the capacitor voltage is equal to the desired voltage. The simulation results of the passivity-based control, the sliding mode control and the passivity-based control combined with sliding mode control demonstrate the effectiveness and show that the capacitor voltage is kept at the desired voltage when the desired voltage, the input voltage E and the load resistor R are changed. The results show that compared with the passivity-based control, the passivity-based control combined with sliding mode control has better performance such as shorter settling time, 8.5 ms when R changes and it has smaller steady-state error, which is indicated by the value of integral absolute error (IAE), 0.0679 when the desired voltage changes. The paper has limitations such as the assumed circuit parameters.**

Keywords—DC-DC Boost Power Converter; Passivity-based Control; Sliding Mode Control.

I. INTRODUCTION

The passivity-based control and its applications to power electronics are investigated by many researchers. A passivity-based control and its applications to the electromechanical applications are presented in [1], [2]. [3] presented the sliding mode control and the passivity-based control. [4] presented the stability of the nonlinear systems using Lyapunov theory, a passivation and a passivity-based control of two-degree of freedom robot. Some passivity-based control approaches were presented in [5]-[8]. A control system for bicycle robot based on a passivity-based method is presented in [6].

A passivity-based control of a DC-DC boost power converter using a generalized PI observer is described in [9] when the time-varying disturbance is included. Moreover, some versions of passivity-based control approaches were presented in [10]-[15]. The passivity-based control of buck-boost converter for different loads research was presented in [13]. The passivity voltage based control of the boost power converter used in photovoltaic (PV) system was described in [16]. The modified passivity-based control methods were presented in [17]-[19]. [20] presented a passivity-based controller for a single-phase rectifier – DC motor system. The advantage of passivity-based control is that the equilibrium point at origin of the plant is asymptotically stable. Therefore, the capacitor voltage is convergent to the desired voltage V_d.

Some nonlinear control approaches of the boost and buck converter were described in [21]-[27]. [23] presented a state-feedback linearization control for output voltage regulation of a DC-DC boost converter with a constant power load. Internal model control of a DC-DC boost converter was presented in [24]. [28] presented the nonlinear cascaded control for a DC-DC boost converter.

Sliding mode control can prevent the capacitor voltage from chattering and it is suitable for the switching plant such as DC-DC boost power converter. Some researches on sliding mode control were presented in [29]-[34]. Estimation based sliding mode control of DC-DC boost converters was presented in [35]. [36] presented fuzzy sliding mode control of DC-DC boost converter with right-half plane zero. Other control methods of dc-dc boost converter such as the adaptive control, robust control and Lyapunov theory were presented in [37]-[39]. [40] presented an adaptive sliding mode control algorithm for boost DC-DC converter of FCHEV. Some improved control schemes and sliding mode control were presented in [41]-[47]. A comparative analysis of conventional and sliding mode control for DC-DC boost converter was presented in [42] for PV system under transient conditions. [45] presented the cascade system control design and stability analysis for a DC-DC boost converter with proportional integral and sliding mode controller and using singular perturbation theory.

Some versions of sliding mode control approaches were presented in [48]-[54]. [53] presented an implementation of sliding mode voltage control controlled buck-boost converter for solar photovoltaic system. A robust sliding mode control of a DC-DC boost converter with switching frequency regulation was presented in [55].

Further, the variations of passivity-based control and its applications were presented [56]-[61]. A passivity-based control using genetic algorithm for a DC-DC boost power converter is proposed in [56]. [59] presented an adaptive passivity-based control of DC-DC buck power converter with constant power load in DC Microgrid systems. The passivity-based sliding mode control for the second-order nonlinear systems was presented in [60]. A method to passivate a given system by using an input-output transformation matrix was described in [62]. Some versions of variations of passivity-based control methods were described in [62]-[68]. [65] presented the passivity-based control combining proportional integral control to improve robustness in DC Microgrids with constant power loads. [66] presented a passive backstepping control of dual active bridge converter in modular three-port DC converter. Passivity-based control combined with sliding mode control can get the advantages of both of control methods, such as the stability, small steady-state error and short settling time.

In this paper, the passivity-based control is combined with the sliding mode control to control a DC-DC boost power converter. Moreover, the passivity-based control for the same converter is also proposed. The simulation results are reported for illustration.

The contribution is

- Another approach of passivity-based control for a DC-DC boost power converter is proposed. It is different from [1], [9].
- Another approach of passivity-based sliding mode control for a DC-DC boost power converter is proposed. It is different from [1], [9], [60]. The sliding mode control law is proposed such that the derivative of Lyapunov function is negative semidefinite. Then the control law is the sum of passivity-based control and sliding mode control.

The paper is organized as follows. First, the introduction is presented in section 1. The dynamical model of a DC-DC boost power converter, its passivity and the passivity-based method are presented in section 2. The design of a passivity-based control combined with the sliding mode control is described in section 3. The simulation results and discussions are described in section 4. Finally, conclusions are presented in section 5.

II. PRELIMINARY AND RESEARCH METHOD

A. Dynamical Model of a DC-DC Boost Power Converter

A DC-DC boost power converter is described in Fig. 1. When the switch is at 2, the current i increases and stores energy in the inductor L. When the switch is at 1, the current i decreases and the energy, which is from the input voltage E and the inductor, stores in the capacitor C (and supplies in the load resistance R). The DC-DC boost power converter has the output voltage which is higher than the input voltage E. The control signal is the duty ratio μ. In practice, the input voltage E can be the output of a rectifier or a photovoltaic system.

The dynamical model [1] of the DC-DC boost power converter in Fig. 1.

$$\begin{cases} \dot{x}_1 = -(1-\alpha)\dfrac{1}{L}x_2 + \dfrac{E}{L} \\ \dot{x}_2 = (1-\alpha)\dfrac{1}{C}x_1 - \dfrac{1}{RC}x_2 \end{cases} \tag{1}$$

Where x_1 is the inductor current i. x_2 is the capacitor voltage v. $\alpha \in \{0,1\}$ is the switch variable (switch position). E>0 is the nominal constant value of the external voltage source. R is the load resistor. L is the inductor. C is the capacitor.

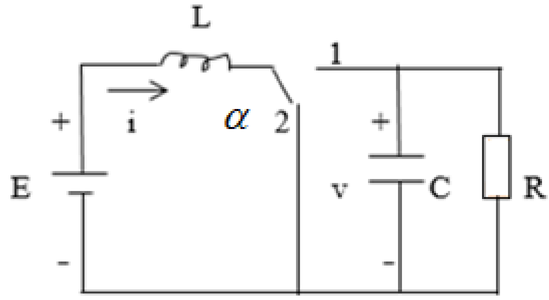

Fig. 1. A DC-DC boost power converter: the inductor L, load resistor R, capacitor C, input voltage E, switch positionα, inductor current i and capacitor voltage v

In [1], an average model of the converter is derived in the following form:

$$\begin{cases} \dot{x}_1 = -(1-\mu)\dfrac{1}{L}x_2 + \dfrac{E}{L} \\ \dot{x}_2 = (1-\mu)\dfrac{1}{C}x_1 - \dfrac{1}{RC}x_2 \end{cases} \tag{2}$$

Where x_1 and x_2 are the corresponding averaged variables. μ is duty ratio. The control input is μ which is continuous and $0 < \mu < 1$. The equilibrium point of (2) is

$$x_{10} = \frac{V_d^2}{ER}; x_{20} = V_d; u_0 = \mu_0 = 1 - \frac{E}{V_d} \tag{3}$$

with $E = 15$ (V), $R = 30$ (Ω), $V_d = 20$ (V). We have x_{10}=0.888, x_{20}=20, μ_0=0.25. E can be the output voltage of a rectifier or a photovoltaic system and E varies. R is the load resistor and R varies. V_d is the desired voltage of the capacitor voltage. Our goal is to regulate the capacitor voltage v at the desired value V_d.

Application: this circuit is used for a rectifier or a photovoltaic system. The DC load and the PV cannot connect directly and the DC-DC boost converter is needed.

B. Passivity-based Method

Definition 1: Consider the dynamical system in the following form:

$$\begin{cases} \dot{x} = f(x,u) \\ y = h(x) \end{cases} \tag{4}$$

Where f is locally Lipschitz, h is continuous; $f\ (0,0) = 0$, and $h\ (0) = 0$.

The plant is passive if there exists a continuously differentiable positive semidefinite function $V(x)$, which is called the storage function, such that

$$u^T y \geq \dot{V} = \frac{\partial V}{\partial x} f(x,u), \qquad \forall (x,u)$$

Definition 2: Consider the plant (4) with $u \equiv 0$. The plant is zero-state observable if $y \equiv 0$ then $x \equiv 0$. Property [3]: Consider the plant (4). If the plant satisfies the following conditions:

i) Passive with a storage function $V(x)$ which is positive semidefinite.

ii) Zero-state observable.

iii) $V(x) \to \infty$ when $x \to \infty$.

Then with the feedback control law $u = -\phi(y)$ with $\phi(0) = 0; y^T\phi(y) > 0 \quad \forall y \neq 0$, the origin achieves global asymptotic stability.

C. Passivity Property of a DC-DC Boost Power Converter

Change the variables as (5).

$$\begin{aligned}\tilde{x}_1 &= x_1 - x_{10} = x_1 - \frac{V_d^2}{ER} \\ \tilde{x}_2 &= x_2 - x_{20} = x_2 - V_d \\ \tilde{u} &= u - u_0 = u - (1 - \frac{E}{V_d})\end{aligned} \tag{5}$$

Note that $\dot{\tilde{x}}_1 = \dot{x}_1; \dot{\tilde{x}}_2 = \dot{x}_2; \tilde{x} = [\tilde{x}_1, \tilde{x}_2]^T$

Inserting (5) into (2), we obtain the state-space equation of the plant

$$\begin{cases} \dot{\tilde{x}}_1 = \dfrac{\tilde{u}}{L}(\tilde{x}_2 + V_d) - \dfrac{E}{LV_d}\tilde{x}_2 \\ \dot{\tilde{x}}_2 = -\dfrac{\tilde{u}}{C}(\tilde{x}_1 + \dfrac{V_d^2}{ER}) + \dfrac{E}{CV_d}\tilde{x}_1 - \dfrac{1}{RC}\tilde{x}_2 \end{cases} \tag{6}$$

The storage function V is chosen as (7)

$$V(\tilde{x}) = \frac{1}{2}\tilde{x}^T \begin{bmatrix} L & 0 \\ 0 & C \end{bmatrix} \tilde{x} = \frac{1}{2}L\tilde{x}_1^2 + \frac{1}{2}C\tilde{x}_2^2 \tag{7}$$

The function V is positive definite. The derivative of V

$$\dot{V} = L\tilde{x}_1\dot{\tilde{x}}_1 + C\tilde{x}_2\dot{\tilde{x}}_2$$

Inserting (6) into $\dot{V}$, we have

$$\begin{aligned}\dot{V} &= L\tilde{x}_1\dot{\tilde{x}}_1 + C\tilde{x}_2\dot{\tilde{x}}_2 \\ &= L\tilde{x}_1\left[\frac{\tilde{u}}{L}(\tilde{x}_2 + V_d) - \frac{E}{LV_d}\tilde{x}_2\right] \\ &+ C\tilde{x}_2\left[-\frac{\tilde{u}}{C}(\tilde{x}_1 + \frac{V_d^2}{ER}) + \frac{E}{CV_d}\tilde{x}_1 - \frac{1}{RC}\tilde{x}_2\right]\end{aligned}$$

$$\begin{aligned}\dot{V} &= \tilde{x}_1\tilde{u}\tilde{x}_2 + V_d\tilde{x}_1\tilde{u} - \frac{E}{V_d}\tilde{x}_1\tilde{x}_2 - \tilde{x}_1\tilde{u}\tilde{x}_2 - \tilde{x}_2\tilde{u}\frac{V_d^2}{ER} \\ &+ \frac{E}{V_d}\tilde{x}_1\tilde{x}_2 - \frac{1}{R}\tilde{x}_2^2 \\ \Rightarrow \dot{V} &= V_d\tilde{x}_1\tilde{u} - \frac{V_d^2}{ER}\tilde{x}_2\tilde{u} - \frac{1}{R}\tilde{x}_2^2 \\ \Rightarrow \dot{V} &= (x_{20}\tilde{x}_1 - x_{10}\tilde{x}_2)\tilde{u} - \frac{1}{R}\tilde{x}_2^2\end{aligned} \tag{8}$$

Let $\tilde{y} = x_{20}\tilde{x}_1 - x_{10}\tilde{x}_2$.

$$\Rightarrow \tilde{y}\tilde{u} = \dot{V} + \frac{1}{R}\tilde{x}_2^2$$

The plant (6), which has the input $\tilde{u}$ and the output $\tilde{y}$, is passive because of $\tilde{y}\tilde{u} \geq \dot{V} + \psi(\tilde{x}) \Rightarrow \tilde{y}\tilde{u} \geq \dot{V}$ with $\psi(\tilde{x}) = \frac{1}{R}\tilde{x}_2^2$. $\psi(\tilde{x})$ is positive semidefinite.

The plant (6) is zero-state observable because $\tilde{u} = 0, \tilde{y} \equiv 0 \Rightarrow \tilde{x}_1 \equiv 0 \Rightarrow \tilde{x}_2 \equiv 0 \Rightarrow \tilde{x} \equiv 0$.

Stability Analysis

We have

$$\begin{aligned}\tilde{y}\tilde{u} \geq \dot{V} + \psi(\tilde{x}) &\Rightarrow \dot{V} \leq \tilde{y}\tilde{u} - \psi(\tilde{x}) \\ &\Rightarrow \dot{V} \leq -\tilde{y}\phi(\tilde{y}) - \psi(\tilde{x}) \leq 0\end{aligned}$$

Therefore, $\dot{V}$ is negative semidefinite.

III. DESIGN THE PASSIVITY-BASED CONTROL COMBINED WITH SLIDING MODE CONTROL

A. Passivity-based Control

According to (6), which satisfies the following conditions in property [3], the control law stabilizes the equilibrium point at origin

$$\tilde{u}_{PBC} = -\phi(\tilde{y}), \phi(0) = 0; \tilde{y}^T\phi(\tilde{y}) > 0 \forall \tilde{y} \neq 0 \tag{9}$$

We can choose

$$\phi(\tilde{y}) = a_1\tilde{y} + a_2\tilde{y}^3 + a_3\tilde{y}^5 \tag{10}$$

The control law is

$$\begin{aligned}u_{PBC} &= -a_1[V_d(x_1 - \frac{V_d^2}{ER}) - \frac{V_d^2}{ER}(x_2 - V_d)] \\ &- a_2[V_d(x_1 - \frac{V_d^2}{ER}) - \frac{V_d^2}{ER}(x_2 - V_d)]^3 \\ &- a_3[V_d(x_1 - \frac{V_d^2}{ER}) - \frac{V_d^2}{ER}(x_2 - V_d)]^5 + (1 - \frac{E}{V_d})\end{aligned} \tag{11}$$

B. Sliding Mode Control

The plant is described in (6). The output is $\tilde{y} = V_d(x_1 - \frac{V_d^2}{ER}) - \frac{V_d^2}{ER}(x_2 - V_d)$. The structure of a sliding mode control is illustrated in Fig. 2.

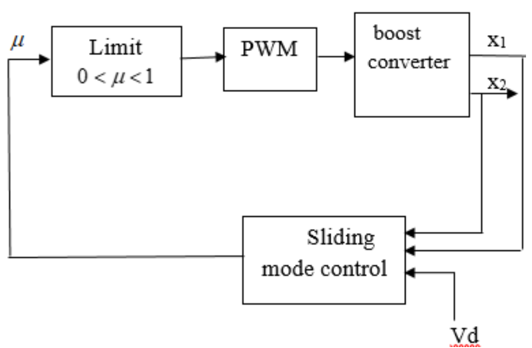

Fig. 2. The structure of sliding mode control for a DC-DC boost power converter: the inductor current x_1, the capacitor x_2, control input μ and desired voltage V_d

The plant (6) is passive with the positive-definite V and is zero-state observable. The function V_b is chosen as (12)

$$V_b = V = \frac{1}{2}L\tilde{x}_1^2 + \frac{1}{2}C\tilde{x}_2^2$$
$$= \frac{1}{2}L(x_1 - \frac{V_d^2}{ER})^2 + \frac{1}{2}C(x_2 - V_d)^2 \tag{12}$$

V_b is positive definite. Choose a sliding surface as (13)

$$S = \tau_1\tilde{y} = \tau_1[V_d(x_1 - \frac{V_d^2}{ER}) - \frac{V_d^2}{ER}(x_2 - V_d)] \tag{13}$$

The derivative of V_b. $\dot{V}_b = \dot{V} \le \tilde{u}\tilde{y}$. For $\dot{V}_b \le 0$, we choose the sliding mode control law as (14)

$$\tilde{u}_{SMC} = -Ksign(\tilde{y}) \tag{14}$$

Where K is a positive constant.

Stability analysis

$V_b = V$ is positive definite.

$$\dot{V}_b = \dot{V} = \tilde{u}\tilde{y} = -Ksign(\tilde{y})\tilde{y} = -K|\tilde{y}|$$
$$\Rightarrow \dot{V}_b = -K|\tilde{y}| \le 0$$

Therefore, $\dot{V}_b$ is negative semidefinite.

C. Passivity-based Control Combined with Sliding Mode Control

The passivity-based control combined with the sliding mode control is (15)

$$\tilde{u} = \tilde{u}_{PBC} + \tilde{u}_{SMC} = -\phi(\tilde{y}) - Ksign(\tilde{y}) \tag{15}$$

Then the control law is (16)

$$\begin{aligned} u = &-a_1[V_d(x_1 - \frac{V_d^2}{ER}) - \frac{V_d^2}{ER}(x_2 - V_d)] \\ &-a_2[V_d(x_1 - \frac{V_d^2}{ER}) - \frac{V_d^2}{ER}(x_2 - V_d)]^3 \\ &-a_3[V_d(x_1 - \frac{V_d^2}{ER}) - \frac{V_d^2}{ER}(x_2 - V_d)]^5 \\ &-Ksign[V_d(x_1 - \frac{V_d^2}{ER}) - \frac{V_d^2}{ER}(x_2 - V_d)] + (1 - \frac{E}{V_d}) \end{aligned} \tag{16}$$

The control signal is the sum of the passivity-based control and the sliding mode control.

Stability Analysis

The plant (6) is rewritten as follows

$$\dot{\tilde{x}} = f(\tilde{x}) + g(\tilde{x})\tilde{u}$$
$$\tilde{y} = x_{20}\tilde{x}_1 - x_{10}\tilde{x}_2$$

Where $\tilde{y}$ is the output of the plant (6),

$$f(\tilde{x}) = \begin{bmatrix} -\frac{E}{LV_d}\tilde{x}_2 \\ \frac{E}{CV_d}\tilde{x}_1 - \frac{1}{RC}\tilde{x}_2 \end{bmatrix}$$

$$g(\tilde{x}) = \begin{bmatrix} \frac{1}{L}(\tilde{x}_2 + V_d) \\ -\frac{1}{C}(\tilde{x}_1 + \frac{V_d^2}{ER}) \end{bmatrix}$$

Let

$$V_2 = V = V_b$$
$$V_2 = V = V_b = \frac{1}{2}L\tilde{x}_1^2 + \frac{1}{2}C\tilde{x}_2^2$$
$$= \frac{1}{2}L(x_1 - \frac{V_d^2}{ER})^2 + \frac{1}{2}C(x_2 - V_d)^2$$

Therefore, the function V_2 is positive definite because of

$$V_2(0,0) = 0; V_2(\tilde{x}_1, \tilde{x}_2) > 0 \forall \tilde{x}_1, \tilde{x}_2 \ne 0.$$

The derivative of V_2

$$\dot{V}_2 = \frac{\partial V_2}{\partial \tilde{x}}\dot{\tilde{x}} = \frac{\partial V}{\partial \tilde{x}}(f(\tilde{x}) + g(\tilde{x})[\tilde{u}_{PBC} + \tilde{u}_{SMC}])$$
$$= \frac{\partial V}{\partial \tilde{x}}(f(\tilde{x}) + g(\tilde{x})\tilde{u}_{PBC}) + \frac{\partial V_b}{\partial \tilde{x}}(f(\tilde{x}) + g(\tilde{x})\tilde{u}_{SMC})$$
$$= \frac{\partial V}{\partial \tilde{x}}(f(\tilde{x}) + g(\tilde{x})(-\phi(\tilde{y})))$$
$$+ \frac{\partial V_b}{\partial \tilde{x}}(f(\tilde{x}) + g(\tilde{x})(-K_1 sign(\tilde{y})))$$

$\dot{V}_2$ is negative semidefinite because $\dot{V} = \frac{\partial V}{\partial \tilde{x}}(f(\tilde{x}) + g(\tilde{x})(-\phi(\tilde{y}))) \le 0$ is negative semidefinite (as indicated in stability analysis of passivity-based control) and $\dot{V}_b = \frac{\partial V_b}{\partial \tilde{x}}(f(\tilde{x}) + g(\tilde{x})(-Ksign(\tilde{y}))) \le 0$ is negative semidefinite (as indicated in stability analysis of sliding mode control). Therefore, the equilibrium point is $\tilde{x}_1 = 0, \tilde{x}_1 = 0, \tilde{u} = 0$ or $x1$, $x2$, u are convergent to $x_{10} = \frac{V_d^2}{ER}; x_{20} = V_d; u_0 = 1 - \frac{E}{V_d}$ respectively. The capacitor voltage v is convergent to the desired value V_d.

IV. SIMULATION AND DISCUSSION

The parameters of the circuits are as follows: $C = 68\mu F$ $L = 0.02\ (H)$, $E = 15\ (V)$, $R = 30\ (\Omega)$, the desired voltage $V_d = 20\ (V)$. The input voltage E varies from 12 (V) to 16.5 (V). The resistance R varies from 15 (Ω) to 40 (Ω). $K = 4$, $\tau_1 = 0.2$. $a_1 = 1.3$, $a_2 = 21.7$, $a_3 = 13$. The simulation time is 0.08 s. Initially, $x1(0) = 0, x2(0) = 0$.

A. Response to the Variations of V_d

At the beginning of the simulation, the desired voltage V_d is set to be 20 (V). At $t = 20$ ms, V_d is decreased to 16 (V) and at $t = 40$ ms, V_d is increased to 18 (V). At $t = 60$ ms, V_d is increased to 20 (V).

1) Passivity-based Control

The PBC results are shown in Fig. 3. Fig. 3 shows the current i, the capacitor voltage v when the system is controlled by the PBC and V_d changes. Fig. 3 shows that at $t = 20$ (ms), when V_d is decreased to 16 (V), the capacitor voltage v has the overshoot, which is indicated by value $\Delta V = |V_d - x_2|$ (V) of 1.012 V. The settling time is equal to 7.5

(ms), and v is equal to 16 (V). At $t = 40$ (ms), when V_d is increased to 18 (V), the capacitor voltage v has ΔV (V) of 0.679 V, and v is equal to 18 (V). At $t = 60$ (ms), when V_d is increased to 20 (V), the capacitor voltage v has the value ΔV (V) of 0.74 V, and v is equal to 20 (V). The value of IAE (integral absolute error (IAE) between V_d and x_2) is 0.0688. IAE is to evaluate the performance quality of the controller. IAE is the sum of the areas below and above the desired voltage V_d and the voltage x_2. $IAE = \int_0^{+\infty} |V_d - x_2| dt$.

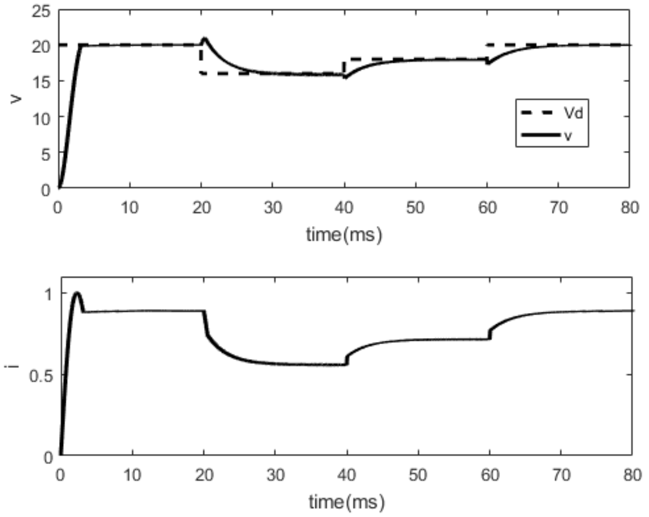

Fig. 3. The results of the PBC when V_d changes: the capacitor voltage v and inductor current i

2) Sliding Mode Control

The SMC results are shown in Fig. 4. Fig. 4 shows the current i, the capacitor voltage v when the system is controlled by the SMC and V_d changes. Fig. 4 shows that at $t = 20$ (ms), when V_d is decreased to 16 (V), the capacitor voltage v has the value ΔV (V) of 1.0818 V. The settling time is equal to 9 (ms), and v is equal to 16 (V). At $t = 40$ (ms), when V_d is increased to 18 (V), the capacitor voltage v has ΔV (V) of 0.391 V and v is equal to 18 (V). At $t = 60$ (ms), when V_d is increased to 20 (V), the capacitor voltage v has the value ΔV (V) of 0.535 V, and v is equal to 20 (V). The value of IAE is 0.0679.

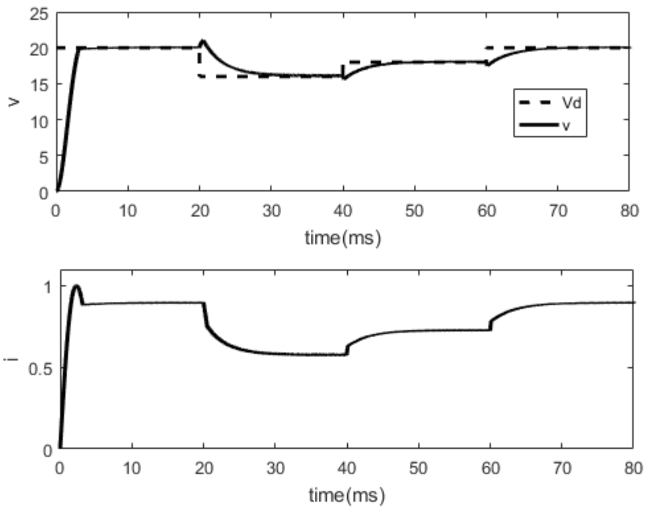

Fig. 4. The results of the SMC when V_d changes: the capacitor voltage v and inductor current i

3) Passivity-based Control Combined with Sliding Mode Control

The PBC-SMC results are shown in Fig. 5. Fig. 5 shows the current i, the capacitor voltage v when the system is controlled by the PBC-SMC and V_d changes. Fig. 5 shows that at $t = 20$ (ms), when V_d is decreased to 16 (V), the capacitor voltage v has the value ΔV (V) of 1.0813 V. The settling time is equal to 8.5 (ms), and v is equal to 16 (V). At $t = 40$ (ms), when V_d is increased to 18 (V), the capacitor voltage v has ΔV (V) of 0.39 V and v is equal to 18 (V). At $t = 60$ (ms), when V_d is increased to 20 (V), the capacitor voltage v has the value ΔV (V) of 0.53 V, and v is equal to 20 (V). The value of IAE is 0.0679.

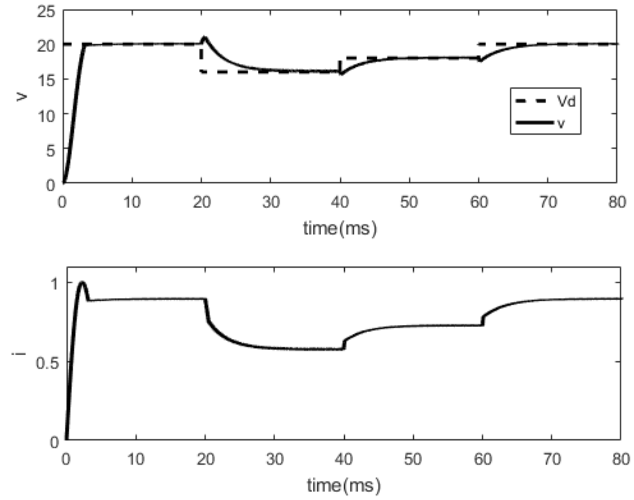

Fig. 5. The results of the PBC-SMC when V_d changes: the capacitor voltage v and inductor current i

When V_d is decreased to 16 (V), the ΔV (V) of the proposed PBC-SMC, 1.0813 V, is larger than that of PBC, 1.012 V. When V_d is increased to 18 (V), the ΔV (V) of the proposed PBC-SMC, 0.39 V, is smaller than that of PBC, 0.679 V. When V_d is increased to 20 (V), the ΔV (V) of the proposed PBC-SMC, 0.53 V, is smaller than that of PBC, 0.74 V. The settling time of PBC, 7.5 ms, is smaller than that of PBC-SMC, 8.5 ms when V_d changes. The IAE of the proposed PBC-SMC, 0.0679, is smaller than that of PBC, 0.0688. Therefore, the results show that the proposed PBC-SMC provides less steady-state error when V_d changes and it has smaller overshoot when V_d is increased to 18 V and 20V. The PBC provides shorter settling time.

The results show that compared with the PBC, the proposed PBC-SMC has smaller steady-state error, which is indicated by IAE, 0.0679 when V_d changes and it has smaller overshoot, which is indicated by ΔV (V), when V_d is increased to 18 V and 20V. However, the PBC has shorter settling time than the PBC-SMC when V_d changes. The results show that compared with the SMC, the PBC-SMC provides shorter settling time and smaller overshoot than the SMC. The PBC-SMC has the same IAE, 0.0679, as the SMC. The comparison results are described in Table I.

It is convenient to combine the PBC method and the SMC method because it can improve the performance, such as short settling time of the PBC and small overshoot of the SMC.

TABLE I. THE CAPACITOR VOLTAGE V WHEN V_D VARIES

Controller	Decreasing V_d (-4 V)		Increasing V_d (+2 V)		Increasing V_d (+2 V)	
	ΔV (V)	t_s (ms)	ΔV (V)	t_s (ms)	ΔV (V)	t_s (ms)
PBC	1.012	7.5	0.679	7.5	0.74	7.5
SMC	1.0818	9	0.391	9	0.535	9
PBC-SMC	1.0813	8.5	0.39	8.5	0.53	8.5

B. Response to the Variations of R

At the beginning of the simulation, the load resistor R is set to be 30 (Ω). At $t = 20$ ms, R is increased to 40 (Ω) and at $t = 40$ ms, R is decreased to 20 (Ω). At $t = 60$ ms, R is increased to 30 (Ω).

1) Passivity-based Control

Fig. 6 is the simulation results of PBC methods when R changes. Fig. 6 shows the current i, the capacitor voltage v and the resistor R. Fig. 6 shows that at $t = 20$ (ms), when R is increased to 40 (Ω), the capacitor voltage v has the value ΔV (V) of 2.12 V. The settling time is equal to 8 (ms), and v is equal to 20 (V). At $t = 40$ (ms), when R is decreased to 20 (Ω), the capacitor voltage v has ΔV (V) of 5.358 V and v is equal to 20 (V). At $t = 60$ (ms), when R is increased to 30 (Ω), the capacitor voltage v has the value ΔV (V) of 4.51 V, and v is equal to 20 (V). The value of IAE is 0.0758.

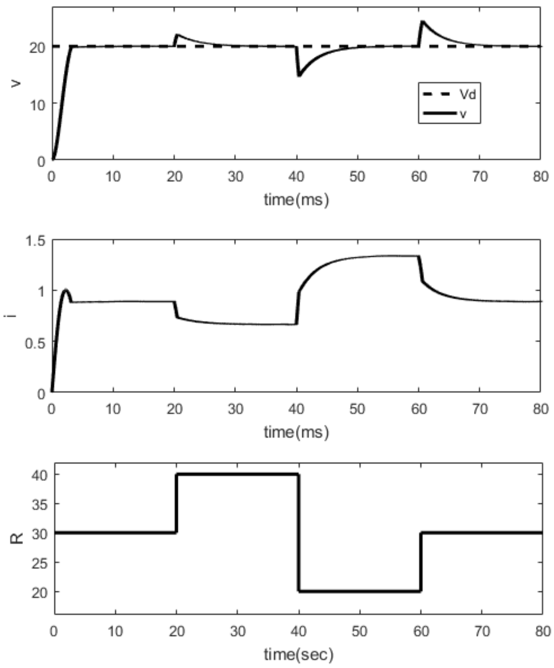

Fig. 6. The results of the PBC when R changes: the capacitor voltage v and inductor current i and load resistor R

2) Sliding Mode Control

Fig. 7 is the simulation results of SMC methods when R changes. Fig. 7 shows the current i, the capacitor voltage v and the resistor R.

Fig. 7 shows that at $t = 20$ (ms), when R is increased to 40 (Ω), the capacitor voltage v has the value ΔV (V) of 2.191 V. The settling time is equal to 10 (ms), and v is equal to 20 (V). At $t = 40$ (ms), when R is decreased to 20 (Ω), the capacitor voltage v has ΔV (V) of 5.4 V and v is equal to 20 (V). At $t = 60$ (ms), when R is increased to 30 (Ω), the capacitor voltage v has the value ΔV (V) of 4.553 V, and v is equal to 20 (V). The value of IAE is 0.0789.

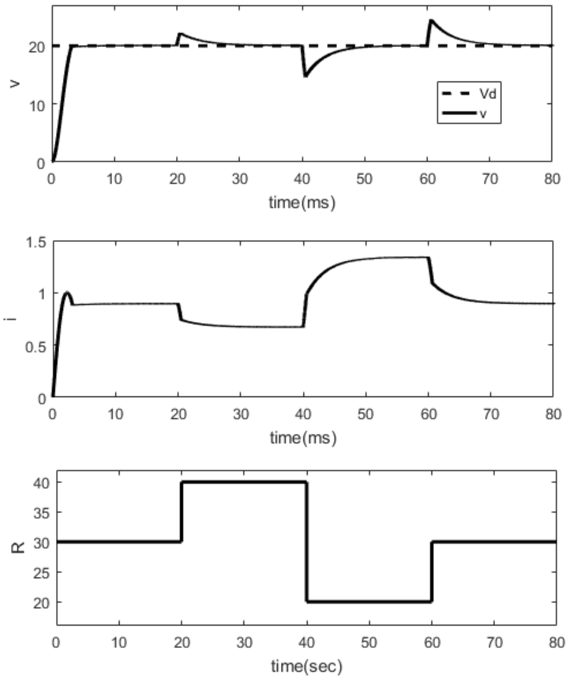

Fig. 7. The results of the SMC when R changes: the capacitor voltage v and inductor current i and load resistor R

3) Passivity-based Control Combined with Sliding Mode Control

Fig. 8 is the simulation results of PBC-SMC methods when R changes. Fig. 8 shows the current i, the capacitor voltage v and the resistor R.

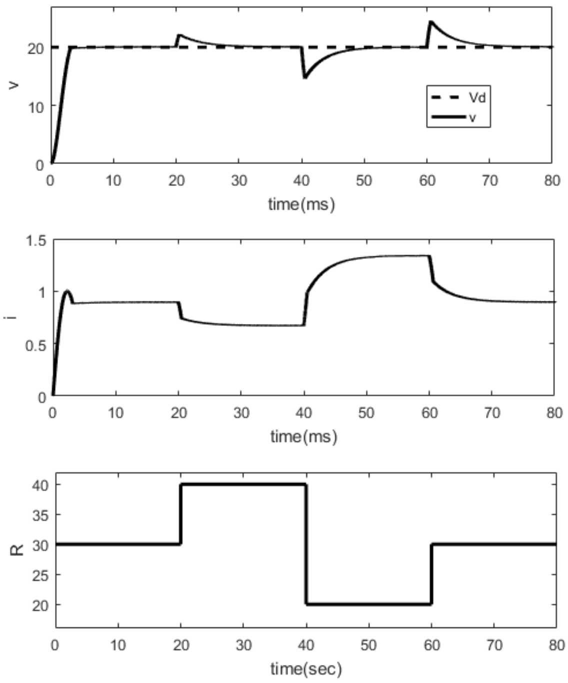

Fig. 8. The results of the PBC-SMC when R changes: the capacitor voltage v and inductor current i and load resistor R

Fig. 8 shows that at $t = 20$ (ms), when R is increased to 40 (Ω), the inductor current i is equal to 0.672 (A). At $t =$ 40 (ms), when R is decreased to 20 (Ω), the inductor current

i is equal to 1.34 (A). At $t = 60$ (ms), when R is increased to 30 (Ω), the inductor current i is equal to 0.895 (A). At $t = 20$ (ms), when R is increased to 40 (Ω), the capacitor voltage v has the value ΔV (V) of 2.19 V. The settling time is equal to 8.5 (ms), and v is equal to 20 (V). At $t = 40$ (ms), when R is decreased to 20 (Ω), the capacitor voltage v has ΔV (V) of 5.4 V and v is equal to 20 (V). At $t = 60$ (ms), when R is increased to 30 (Ω), the capacitor voltage v has the value ΔV (V) of 4.5 V, and v is equal to 20 (V). The value of IAE is 0.0789.

When R is increased to 40 (Ω), the ΔV (V) of the proposed PBC-SMC, 2.19 V, is larger than that of PBC, 2.12 V. When R is decreased to 20 (Ω), the ΔV of the proposed PBC-SMC, 5.4 V, is larger than that of PBC, 5.358 V. When R is increased to 30 (Ω), the ΔV of the proposed PBC-SMC, 4.5 V, is smaller than that of PBC, 4.51 V. The settling time of PBC-SMC, 8.5 ms, is smaller than that of PBC, 8.8 ms or 9 ms when R changes. The IAE of the proposed PBC-SMC, 0.0789 is larger than that of PBC, 0.0758. Therefore, the results show that the proposed PBC provides less steady-state error when R changes and it has smaller overshoot when R is increased to 40 Ω and R is decreased to 20 Ω. The proposed PBC-SMC provides shorter settling time.

The results show that compared with PBC, the proposed PBC-SMC has shorter settling time than the PBC when R changes. However. the PBC provides smaller steady-state error when R changes and it has smaller overshoot when R is increased to 40 Ω and R is decreased to 20 Ω. The PBC-SMC provides shorter settling time than SMC. The PBC-SMC provides the same IAE, 0.0789, as the SMC. The comparison results are described in Table II. The PBC-SMC method can prevent the capacitor voltage v from chattering.

TABLE II. THE CAPACITOR VOLTAGE V WHEN R VARIES

Controller	Increasing R (+10Ω)		Decreasing R (-20Ω)		Increasing R (+10Ω)	
	ΔV (V)	t_s (ms)	ΔV (V)	t_s (ms)	ΔV (V)	t_s (ms)
PBC	2.12	8.8	5.358	8.8	4.51	9
SMC	2.191	10	5.4	10	4.553	10
PBC-SMC	2.19	8.5	5.4	8.5	4.5	8.5

C. Response to the Variations of E

At the beginning of the simulation, the input voltage E is set to be 15 (V). At $t = 20$ ms, E is increased to 16.5 (V) and at $t = 40$ ms, E is decreased to 13.5 (V). At $t = 60$ ms, E is increased to 15 (V).

1) Passivity-based Control

Fig. 9 is the simulation results of PBC method when E changes. Fig. 9 shows the current i, the capacitor voltage v and the input voltage E. Fig. 9 shows that at $t = 20$ (ms), when E is increased to 16.5 (V), the capacitor voltage v has the value ΔV (V) of 0.75 V. The settling time is equal to 6 (ms), and v is equal to 20 (V). At $t = 40$ (ms), when E is decreased to 13.5 (V), the capacitor voltage v has ΔV (V) of 1.55 V and v is equal to 20 (V). At $t = 60$ (ms), when E is increased to 15 (V), the capacitor voltage v has the value ΔV (V) of 0.95 V, and v is equal to 20 (V). The value of IAE is 0.0454.

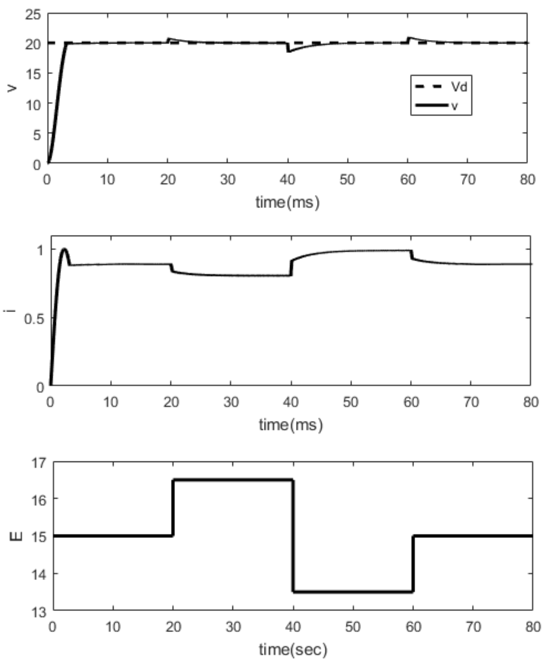

Fig. 9. The results of the PBC when E changes: the capacitor voltage v and inductor current i and input voltage E

2) Sliding Mode Control

Fig. 10 is the simulation results of SMC methods when E changes. Fig. 10 shows the current i, the capacitor voltage v and the input voltage E. Fig. 10 shows that at $t = 20$ (ms), when E is increased to 16.5 (V), the capacitor voltage v has the value ΔV (V) of 0.824 V. The settling time is equal to 7 (ms) and v is equal to 20 (V). At $t = 40$ (ms), when E is decreased to 13.5 (V), the capacitor voltage v has ΔV (V) of 1.47 V and v is equal to 20 (V). At $t = 60$ (ms), when E is increased to 15 (V), the capacitor voltage v has the value ΔV (V) of 0.955 V and v is equal to 20 (V). The value of IAE is 0.0477.

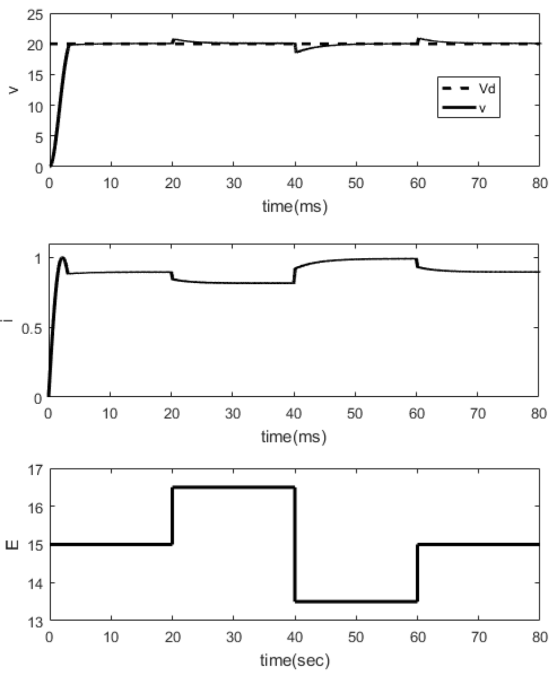

Fig. 10. The results of the SMC when E changes: the capacitor voltage v and inductor current i and input voltage E

3) Passivity-based Control Combined with Sliding Mode Control

Fig. 11 is the simulation results of PBC-SMC methods when E changes. Fig. 11 shows the current i, the capacitor voltage v and the input voltage E. Fig. 11 shows that at $t = 20$ (ms), when E is increased to 16.5 (V), the inductor current i is equal to 0.815 (A). At $t = 40$ (ms), when E is decreased to 13.5 (V), the inductor current i is equal to 0.992 (A). At $t = 60$ (ms), when E is increased to 15 (V), the inductor current i is equal to 0.896 (A). At $t = 20$ (ms), when E is increased to 16.5 (V), the capacitor voltage v has the value ΔV (V) of 0.82 V. The settling time is equal to 6.5 (ms), and v is equal to 20 (V). At $t = 40$ (ms), when E is decreased to 13.5 (V), the capacitor voltage v has ΔV (V) of 1.45 V, and v is equal to 20 (V). At $t = 60$ (ms), when E is increased to 15 (V), the capacitor voltage v has the value ΔV (V) of 0.925 V, and v is equal to 20 (V). The value of IAE is 0.0477.

When E is increased to 16.5 (V), the ΔV (V) of the proposed PBC-SMC, 0.82 V, is larger than that of PBC, 0.75 V. When E is decreased to 13.5 (V), the ΔV of the proposed PBC-SMC, 1.45 V, is smaller than that of PBC, 1.55 V. When E is increased to 15 (V), the ΔV of the proposed PBC-SMC, 0.925 V, is smaller than that of PBC, 0.95 V. The settling time of PBC, 6 ms, is smaller than that of PBC-SMC, 6.5 ms or 6.7 ms when E changes.

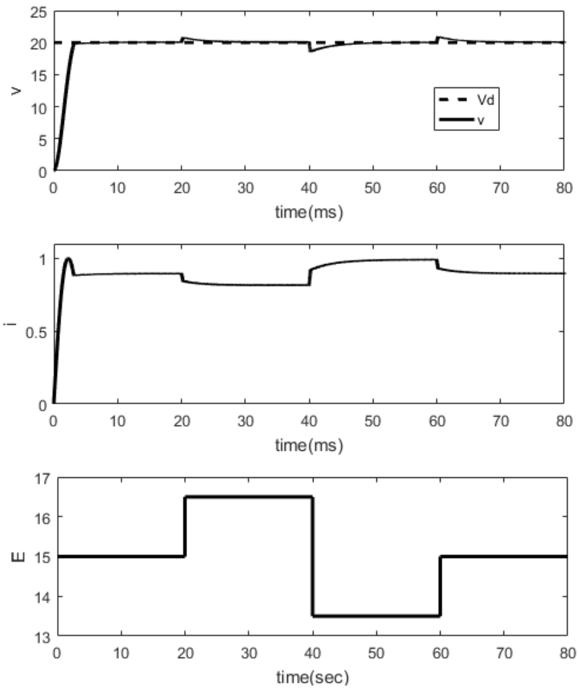

Fig. 11. The results of the PBC-SMC when E changes: the capacitor voltage v and inductor current i and input voltage E

The IAE of the PBC, 0.0454, is smaller than that of PBC-SMC, 0.0477. Therefore, the results show that the PBC provides less steady-state error, and shorter settling time. The PBC-SMC provides smaller overshoot when E is decreased to 13.5 (V), and E is increased to 15 (V).

The results show that compared with the PBC-SMC, the proposed PBC has smaller steady-state error and shorter settling time when E changes. However, the proposed PBC-SMC has smaller overshoot than the PBC when E is decreased to 13.5 (V) and E is increased to 15 (V). The results show that compared with the SMC, the PBC-SMC provides shorter settling time, and smaller overshoot than the SMC. The PBC-SMC provides the same IAE, 0.0477, as the SMC. The comparison results are described in Table III.

TABLE III. THE CAPACITOR VOLTAGE V WHEN E VARIES

Controller	Increasing E (+1.5V)		Decreasing E (-3V)		Increasing E (+1.5V)	
	ΔV (V)	t_s (ms)	ΔV (V)	t_s (ms)	ΔV (V)	t_s (ms)
PBC	0.75	6	1.55	6	0.95	6
SMC	0.824	7	1.47	7	0.955	7
PBC-SMC	0.82	6.5	1.45	6.5	0.925	6.7

V. CONCLUSION

In this paper, the passivity-based control combined with sliding mode control for a DC-DC boost power converter is proposed. Additionally, a standalone passivity-based control strategy for the same converter is proposed. The simulation results of the PBC, the SMC and the PBC-SMC are done with Simulink in MATLAB. The simulations results are performed in three cases of the desired voltage V_d changing, the input voltage variations, E, and the load resistor variation, R. Stability analysis of the PBC-SMC proves that the equilibrium point at origin of the plant (6) is asymptotically stable. Therefore, the inductor current i and the capacitor voltage v are convergent to $\frac{V_d^2}{ER}$, V_d respectively. The simulation results show that the capacitor voltage v is kept at desired value V_d when the desired voltage V_d, the input voltage E and the load resistor R are changed. The results, conducted under varying conditions of V_d, R and E, demonstrate the effectiveness of the proposed passivity-based control and the passivity-based control combined with sliding mode control. The simulation results show that compared with the PBC-SMC, the PBC has smaller steady-state error, which is indicated by the value of IAE, 0.0758, when R changes and it has smaller overshoot indicated by $\Delta V$when R is increased to 40 Ω and R is decreased to 20 Ω. However, the proposed PBC-SMC has shorter settling time, 8.5 ms than the PBC when R changes. Additionally, the results show that compared with the PBC, the proposed PBC-SMC has smaller steady-state error, which is indicated by IAE, 0.0679, when V_d changes and it has smaller overshoot when V_d is increased to 18 V and 20V. However, the PBC displays shorter settling time, 7.5 ms than the PBC-SMC when V_d changes. Further, the results show that compared with the PBC-SMC, the PBC provides smaller steady-state error and shorter settling time when E changes. However, it's worth noting that the proposed PBC-SMC outperforms the PBC in terms of overshoot when E is decreased to 13.5 (V) and E is increased to 15 (V). Moreover, the proposed PBC has the least value of IAE against variations of R and E. The insights from our study suggest that passivity-based control combined with sliding mode control can improve the performance of DC-DC boost power converters, particularly in scenarios where quick responses to voltages variations are crucial. However, the choice of control strategy may need to be tailored to the specific requirements of the systems. The paper has limitations such as the assumed circuit parameters. Future research will explore a practical real-time experiments. The parameters of the passivity-based control are adjusted optimally. In conclusion, our study offers valuable contributions to the field of power electronics control. By demonstrating the advantages and trade-offs of different control strategies, we hope to inspire further research and innovation in the design and optimization of DC-DC boost power converters for a wide range of applications.

ACKNOWLEDGMENT

We acknowledge the support of time and facilities from Ho Chi Minh City University of Technology (HCMUT), VNU-HCM for this study.

ABBREVIATIONS

PBC : Passivity-based Control.

SMC : Sliding Mode Control.

PBC-SMC : Passivity-based Control-Sliding Mode Control.

REFERENCES

[1] R. Ortega, A. Loria, P. J. Nicklasson, and H. Sira-Ramirez. *Passivity-based control of Euler-Lagrange systems*. London: Springer-Verlag, 1998.

[2] E. Rodriguez, R. Leyva, G. G. Farivar, H. D. Tafti, C. D. Townsend, and J. Pou, "Incremental passivity control in multilevel cascaded H-Bridge converters," *IEEE Transactions on Power electronics*, vol. 35, no. 8, pp. 8766-8778, 2020, doi: 10.1109/TPEL.2020.2965164.

[3] H. N. Duong. *Control of MIMO systems*. Ho Chi Minh City: VNU Press, 2013.

[4] H. K. Khalil. *Nonlinear systems*. New Jersey: Prentice-Hall 3rd edition, 2002.

[5] M. Li, G. Chesi, and Y. Hong, "Input-Feedforward-passivity-based distributed optimization over jointly connected balanced digraphs," *IEEE Transactions on Automatic Control*, vol. 66, no. 9, pp. 4117-4131, 2021, doi: 10.1109/TAC.2020.3028838.

[6] M. N. Huynh, H. N. Duong, and V. H. Nguyen, "Passivity-based control of bicycle robot," *VNUHCM Journal of Engineering and Technology*, vol. 5, no. 2, pp. 1520-1527, 2022, doi: 10.32508/stdjet.v5i2.954.

[7] V. Krishnamurthy and G. Yin, "Multikernel passive stochastic gradient algorithms and transfer learning," *IEEE Transactions on Automatic control*, vol. 67, no. 4, pp. 1792-1805, 2022, doi: 10.1109/TAC.2021.3079280.

[8] S. Monaco, D. Normand-Cyrot, M. Mattioni, and A. Moreschini, "Nonlinear hamiltonian systems under sampling," *IEEE Transactions on Automatic control*, vol. 67, no. 9, pp. 4598-4613, 2022, doi: 10.1109/TAC.2022.3164985.

[9] W. He, S. Li, J. Yang, and Z. Wang, "Incremental passivity-based control for dc-dc boost converter under time-varying disturbances via a generalized proportional integral observer," *Journal of Power Electronics*, vol. 18, no. 1, pp. 147-159, 2018.

[10] W.J. Gil-Gonzalez, O.D. Montoya, A. Garces, F.M. Serra, and G. Magaldi, "Output voltage regulation for dc-dc buck converter: a passivity-based PI design," in *2019 IEEE 10th Latin American Symposium on circuits and systems (LASCAS)*, pp. 189-192, 2019, doi: 10.1109/LASCAS.2019.8667557.

[11] W. Li, K. Qin, B. Chen, and M. Shi, "Passivity-based distributed tracking control of uncertain agents via a neural network combined UDE," *Journal of Neurocomputing*, vol. 449, pp. 342-356, 2021, doi: 10.1016/j.neucom.2021.03.008.

[12] E. Nuno and R. Ortega, "Achieving consensus of euler-lagrange agents with interconnecting delays and without velocity measurements via passivity-based control," *IEEE Transactions on Control systems Technology*, vol. 26, no. 1, pp. 222-232, 2018, doi: 10.1109/TCST.2017.2661822.

[13] F. Zhang *et al*., "Passivity-based control of buck-boost converter for different loads research," *Journal of Electrical and Computer Engineering*, vol. 2023, 2023, doi: 10.1155/2023/5558246.

[14] M. Sharf, A. Jain, and D. Zelazo, "Geometric method for passivation cooperative control of equilibrium—independent passive-sgort systems," *IEEE Transactions on Automatic control*, vol. 66, no. 12, pp. 5877-4892, 2021, doi: 10.1109/TAC.2020.3043390.

[15] A. Turnwald, M. Schäfer, and S. Liu, "Passivity-Based Trajectory Tracking Control for an Autonomous Bicycle," *IECON 2018 - 44th Annual Conference of the IEEE Industrial Electronics Society*, pp. 2607-2612, 2018, doi: 10.1109/IECON.2018.8591382.

[16] K. Baazouzi, A.D. Bensalah, S. Drid, and L. Chrifi-Alaoui, "Passivity voltage based control of the boost power converter used in photovoltaic system," *Electrical Engineering and Electromechanics*, vol. 2, pp. 11-17, 2022, doi: 10.20998/2074-272X.2022.2.02.

[17] M. Ahmed, A. Elhassane, and A. Mohamed, "Modelling and passivity-based control of a non isolated dc-dc converter in fuel cell system," *International Journal of Electrical and Computer Engineering (IJECE)*, vol. 8, no. 5, pp. 3436-3443, 2018, doi: 10.1159/ijece.v8i5. pp 3436-3443.

[18] J. Kong, "Modified passivity-based control method for three phase cascaded unidirectional multilevel converters," *Journal of Power Electronics*, vol. 23, pp. 1185-1195, 2023, doi: 10.1007/s43236-023-00615-1.

[19] E. Moreno-Negrete, C. F. Mendez-Barrios, and D. Langarica-Cordoba, "On the PI-PBC controllers for a high gain transformerless dc-dc converter," in *Advances in Automation and Robotics Research: Proceedings of the 3rd Latin American Congress on Automation and Robotics, Monterrey, Mexico 2021*, pp. 261-269, 2022, doi: 10.1007/978-3-Q30-90033-5_28.

[20] R. Heredia-Barba, J. A. Juarez-Abad, J. Linares-Flores, M. A. Contreras-Ordaz, and J. L. Barahona-Avalos, "Passivity-based controller for a high energy quality active rectifier-DC motor system: an FPGA implementation," *Journal of Power Electronics*, vol. 23, pp. 666-676, 2023, doi: 10.1007/s43236-022-00563-2.

[21] M. Malekzadeh, A. Khosravi, and M. Tavan, "An immersion and invariance based input voltage and resistive load observer dc-dc boost converter," *SN Applied Sciences*, vol. 2, 78, 2020, doi: 10.1007/s42452-019-1880-7.

[22] Z. J. Yegane and A. Asghari, "A new high step-up dc/dc converter based on integrating coupled-inductor and voltage multiplier cell techniques for renewable energy applications," in *2020 11th Power Electronics, Drive systems, and Technologies Conference (PEDSTC)*, pp. 1-6, 2020, doi: 10.1109/PEDSTC49159.2020.9088475.

[23] B. A. Martinez-Trevino, A. E. Aroudi, A. Cid-Pastor, and L. Martinez-Salamero, "Nonlinear control for output voltage regulation of a boost converter with a constant power load," *IEEE Transactions on Power Electronics*, vol. 34, no. 11, pp. 10381-10385, 2019, doi: 10.1109/TPEL.2019.2913570.

[24] P. Verma, Md. N. Anwar, M. K. Ram, and A. Iqbal, "Internal model control scheme - based voltage and current mode control of dc-dc boost converter," *IEEE Access*, vol. 11, pp. 110558-110569, 2023, doi: 10.1109/ACCESS.2023.3320272.

[25] M. Mohadeszadeh, N. Pariz, and M.R. Ramezanial, "A fractional reset control scheme for a dc-dc buck converter," *International Journal of Dynamics and Control*, vol. 10, pp. 2139-2150, 2022, doi: 10.1007/s40435-022-00928-2.

[26] M. K. Sameer Kumar, J. Day, and R. Mondal, "Fractional-order (fo) control of dc-dc buck-boost converter," In *Advances in Power and Control Engineering: Proceedings of GUCON 2019*, pp. 107-117, 2020, doi: 10.1007/978-981-15-0313-9_8.

[27] A. Marahatta, Y. Rajbhandari, A. Shrestha, S. Phuyal, A. Thapa, and P. Korba, "Model predictive control of dc/dc boost converter with reinforcement learning," *Journal of Heliyon*, vol. 8, no. 11, 2022, doi: 10.1016/j.heliyon.2022.e11416.

[28] A. Mansouri, R. Gavagsaz-Ghoachani, M. Phattanasak, and S. Pierfederici, "Nonlinear cascaded control for a dc-dc boost converter," *Journal of Robotics and Control (JRC)*, vol. 4, no. 4, 2023, doi: 10.18196/jrc.v4i4.18932.

[29] S. J. Gambhire, D. R. Kishore, P. S. Londhe, and S. N. Pawar, "Review of sliding mode based control techniques for control system

applications," *International Journal of Dynamics and Control*, vol. 9, pp. 363-378, 2021, doi: 10.1007/s40435-020-00638-7.

[30] B. Taheri, M. Sedaghat, M. A. Bagherpour, and P. Farhadi, "A new controller for dc-dc converters based on sliding mode control techniques," *Journal of Control, automation and electrical systems*, vol. 30, pp. 63-74, 2019, doi: 10.1007/s40313-018-00427-w.

[31] J. Qiu, W. Ji, and M. Chadli, "A novel fuzzy output feedback dynamic siding mode controller design for two-dimensional nonlinear systems," *IEEE Transaction on Fuzzy systems*, vol. 29, no. 10, pp. 2869-2877, October 2021, doi: 10.1109/TFUZZ.2020.3008271.

[32] K. K. Panday, M. Kumar, A. Kumari, and J. Kumar, "Bidirectional dc-dc buck-boost converter for battery energy storage system anfd pv panel," In *Modeling, Simulation and Optimization: Proceedings of CoMSO 2020*, pp. 681-693, 2021, doi: 10.1007/978-981-15-9829-6_54.

[33] J. E. Ruiz-Duarte and A. G. Loukianov, "Sliding mode output-feedback causal output tracking for a class of discrete-time nonlinear systems," *International Journal of Robust and nonlinear control*, vol. 29, no.6, pp. 1956-1975, April 2019, doi: 10.1002/rnc.4470.

[34] I. O. Aksu and R. Coban, "Sliding mode PI control with backstepping approach for MIMO nonlinear cross-coupled tank systems," *International Journal of Robust and nonlinear control*, vol. 29, no.6, pp. 1854-1871, April 2019, doi: 10.1002/rnc.4469.

[35] T. T. Sarkar and C. Mahanta, "Estimation based sliding mode control of dc-dc boost converters," *Journal of IFAC-PapersOnline*, vol. 55, no. 1, pp. 467-472, 2022, doi: 10.1016/j.ifacol.2022.04.077.

[36] T. Anitha, B. Rajagopal, and S. Arulselvi, "Fuzzy sliding mode control of dc-dc boost converter with right-half plane zero," in *Artificial Intelligence and Evolutionary Computations in Engineering Systems: Computational Algorithm for AI Technology, Proceedings of ICAIECES 2020*, pp. 95-111, 2022, doi: 10.1007/978-981-16-2674-6_8.

[37] K. Raman, K. Jeyaraman, S. Mekhilef, and L. G. Alexander, "Design and stability analysis of interleaved flyback converter using Lyapunov direct method with FPGA implementation," *Journal of Electrical engineering*, vol. 102, pp. 1651-1665, 2020, doi: 10.1007/s00202-020-00976-x.

[38] Z. Alam, S. K. Ghosh, A. F. Alkhateeb, T. K. Roy, M. S. Islam, S. Saha, and M. A. Hussain, "Robust hybrid nonlinear control approach for stability enhancement of a constant power load boost converter," *Alexandria Engineering Journal*, vol. 74, pp. 535-545, 2023, doi: 10.1016/j.aej.2023.05.041.

[39] X. Wang, W. He, and T. Li, "An adaptive observer for sensorless current control of boost converter feeding unknown constant power load," In *Chinese Intelligent Automation Conference*, pp. 830-837, 2023, doi: 10.1007/978-981-99-6187-0_83.

[40] Y. Wang, S. Song, L. Zhu, and Z. Fu, "An adaptive sliding mode control algorithm for boost dc-dc converter of fchevs," in *ICNCC'19 Proceedings of the 2019 8th International Conference on Networks, Communication, and computing*, pp. 212-216, 2019, doi: 10.1145/3375998.3376021.

[41] A. Gupta and D. Joshi "Comparative analysis of nonlinear smc controller with linear pid controller for flyback converter," *DC—DC Converters for Future Renewable Energy Systems*, pp. 71-87, 2022, doi: 10.1007/978-981-16-4388-0.

[42] B. Swarnkar, S. K. Gawre, and G. Akodiya, "Comparative analysis of conventional and sliding mode control techniques for DC-DC boost converter for PV system under transient conditions," in *Recent Advances in Power Electronics and Drives: Select Proceedings of EPREC 2021*, pp. 587-600, 2022, doi: 10.1007/978-981-16-9239-0_45.

[43] M. J. Daylamani, P. Amiri, and M. H. Refan, "Design and stability analysis of a discrete-time sliding mode control for a synchronous dc-dc buck converter," *International Journal of Control, automation and systems*, vol. 17, pp. 1393-1407, 2019, doi: 10.1007/s12555-017-9793-y.

[44] T. R. Burle, G. Satpathy, and D. De, "Hybrid controller configuration for master-slave paralleling of dc-dc converters with improved sliding manifold," *Electrical engineering*, pp. 1-13, 2023, doi: 10.1007/s00202-023-01976-3.

[45] S. Azarastemal and M. Hejri, "Cascade control system design and stability analysis of a dc-dc boost converter with proportional integral and sliding mode controller and using singular perturbation theory," *Iranian Journal of Science and Technology, Transactions of Electrical engineering*, vol. 45, pp. 1445-1462, July 2021, doi: 10.1007/s40998-021-00444-7.

[46] A. Goudarzian and A. Khosravi, "A unified method to the design of an improved high frequency sliding mode current controller for dc/dc boost converter in continuous current condition based on analogue implementation," *Sadhana*, vol. 45, 281, 2020, doi: 10.1007/s12046-020-01507-x.

[47] M. K. Kanthi and A. D. Mary, "Performance analysis of sliding mode controlled bidirectional dc-dc converter for electric vehicles," *Smart Sensors Measurements and Instrumentation: Select Proceedings of CISCON 2020*, pp. 335-349, 2021, doi: 10.1007/978-981-16-0336-5_28.

[48] A. Singh and A. Ghosh, "Comparison of quantitative feedback theory dependent controller with conventional PID and sliding mode controllers on dc-dc boost converter for microgrid applications," *Technology and Economics of Smart Grids and sustainable energy*, vol. 7, no. 11, 2022, doi: 10.1007/s40866-022-00133-2.

[49] Z. Elhajji, K. Dehri, Z. Bouchama, A. S. Nouri, and N. Essounbouli, "Robustness analysis of a discrete integral sliding mode controller for dc-dc buck converter using input-output measurement," In *Advances in Robust Control and Applications*, pp. 273-284, 2023, doi: 10.1007/978-981-99-3463-8_11.

[50] L. Zhou, X. Yi, J. She, and Z. Zhang, "Generalized extended state observer based sliding mode control for buck converter systems," *International Journal of Control, automation and systems*, vol. 20, pp. 3923-3931, 2022, doi: 10.1007/s12555-021-0382-8.

[51] J. Wu, L. Luo, C. Wen, and Q. Wang, "Inverse decoupling sliding mode control for multilevel buck converter in low power applications," *Journal of Power Electronics*, vol. 23, pp. 1174-1184, 2023, doi: 10.1007/s43236-023-00667-3.

[52] K. A. Singh, S. Soni, A. Sachan, and K Chaudhary, "PWM-based proxy sliding mode controller for DC-DC buck converters," In *Modelling, Simulation and Intelligent Computing: Proceedings of MoSICom 2020*, pp. 365-374, 2020, doi: 10.1007/978-981-15-4775-1_39.

[53] N. A. M. Mustakin, M. Bakar, and M. Noh, "An implementation of sliding mode voltage control controlled buck-boost converter for solar applicaton," In *Advances in Intelligent Manufacturing and Mechatronics: Selected Articles from the Innovative Manufacturing, Mechatronics & Materials Forum (iM3F 2022)*, pp. 53-60, 2023, doi: 10.1007/978-981-19-8703-8_5.

[54] P. P. Arya, "Internal model based dynamic sliding mode control for DC-DC boost converters," *Journal of IFAC-PapersOnline*, vol. 55, no. 1, pp. 567-571, 2022, doi: 10.1016/j.ifacol.2022.04.093.

[55] V. Repecho, D. Biel, J. M. Olm, and E Fossas, "Robust sliding mode control of a dc/dc boost converter with switching frequency regulation," *Journal of the Franklin Institute*, vol. 355, no. 13, pp.5367-5383, 2018, doi: 10.1016/j.jfranklin.2018.05.028.

[56] M. N. Huỳnh, H. N. Dương, and V. H. Nguyễn, "Passivity-based control using genetic algorithm for a DC-DC boost power converter," *VNUHCM Journal of Engineering and Technology*, vol. 6, no. 2, pp. 1891-1905, 2023, doi: 10.32508/stdjet.v6i2.1053.

[57] Q. Xiao, T. Huang, and M. A. Hussain, "Passivity and passification of fuzzy memristive inertial neural networks on time scales," *IEEE Transactions on Fuzzy systems*, vol. 26, no. 6, pp. 3342-3355, 2018, doi: 10.1109/TFUZZ.2018.2825306.

[58] S. Zare, A. R. Tavakolpour-Saleh, and T. Binazadeh, "Passivity-based control technique incorporating genetic algorithm for design of a free piston stirling engine," *Journal of Renewable Energy Focus*, vol. 28, no.0, pp. 66-77, March 2019, doi: 10.1016/j.ref.2018.11.003.

[59] M. A. Hassan, E. Li, X. Li, T. Li, C. Duan, and S. Chi, "Adaptive passivity-based control of dc-dc buck power converter with constant power load in DC Microgrid systems," *IEEE Journal of Emerging and selected topics in power electronics*, vol. 7, no. 3, pp. 2029-2040, 2019, doi: 10.1109/JESTPE.2018.2874449.

[60] J. L. Chang, "Passivity-based sliding mode controller/observer for second-order nonlinear systems," *International Journal of Robust and nonlinear control*, vol. 29, no. 6, pp. 1976-1989, 2019, doi: 10.1002/rnc.4474.

[61] M. Cucuzzella, R. Lazzari, Y. Kawano, K. C. Kosaraju, and J. M. A. Scherpen, "Robust Passivity-Based Control of Boost Converters in DC

Microgrids⋆," *2019 IEEE 58th Conference on Decision and Control (CDC)*, pp. 8435-8440, 2019, doi: 10.1109/CDC40024.2019.9029657.

[62] M. Xia, A. Rahnama, S. Wang, and P. J. Antsaklis, "Control design using passivation for stability and performance," *IEEE Transactions on Automatic Control*, vol. 63, no. 9, pp. 2987-2993, 2018, doi: 10.1109/TAC.2018.2789681.

[63] W. Liu, X. Cui, J. Zhou, Z. Zhang, M. Hou, S. Shan, and S. Wu, "Composite passivity based control of dc/dc boost converters with constant power loads in dc microgrid," *Journal of Power Electronics*, vol. 22, pp. 1927-1937, 2022, doi: 10.1007/s43236-022-00492-0.

[64] M. T. Vo, V. D. H. Nguyen, H. N. Duong, and V. H. Nguyen, "Combining passivity-based control and linear quadratic regulator to control a rotary inverted pendulum," *Journal of Robotics and Control (JRC)*, vol. 4, no. 4, 2023, doi: 10.18196/jrc.v4i4.18498.

[65] Q. Xian, Y. Wang, F. Wang, R. Li, and S. Wang, "Hybrid passivity-based control for stability and robustness enhancement in dc microgrids with constant power loads," *Journal of Power Electronics*, vol. 23, pp. 296-307, 2023, doi: 10.1007/s43236-022-00529-4.

[66] X. Li and X. Fang, "Passive backstepping control of dual active bridge converter in modular three-port DC converter," *Electronics*, vol. 12, no. 5, p. 1074, 2023, doi: 10.3390/electronics12051074.

[67] B. Said, T. Ilyes, K. Okba, D. E. Zabia, and M. Messaoud, "Optimized passivity-based control of a hybrid electric vehicle source using a novel optimizer," *Electrotehnica, Electronica, Automatica*, vol. 71, no. 3, pp. 23-31, 2023, doi: 10.46904/eea.23.71.3.1108003.

[68] J. Zhou, Q. Zhang, M.A. Hassan, Z. Zhana, M. Hou, S. Wu, Y. Li, E. Li, and J. M. Guerrero, "A robust passivity based model predictive control for buck converter suppling constant power load," *Energy Reports*, vol. 7, no. 7, pp. 792-813, 2021, doi: 10.1016/j.egyr.2021.09.193.